particles

MDPI

Article

A New Measurement of Light Yield Quenching in EJ-200 and LYSO Scintillators

Francesco Dimiccoli [1,2], Francesco Maria Follega [1,2], Luigi Ernesto Ghezzer [1,2], Roberto Iuppa [1,2], Alessandro Lega [1,3], Riccardo Nicolaidis [1,2], Francesco Nozzoli [1,2,*], Ester Ricci [1,3], Enrico Verroi [1] and Paolo Zuccon [1,2]

[1] Istituto Nazionale Fisica Nucleare—TIFPA, Via Sommarive 14, I-38123 Trento, Italy
[2] Department of Physics, University of Trento, Via Sommarive 14, I-38123 Trento, Italy
[3] Fondazione Bruno Kessler, Via Sommarive 18, I-38123 Trento, Italy
* Correspondence: francesco.nozzoli@unitn.it

Abstract

Lutetium–Yttrium Oxyorthosilicate (LYSO) crystals and EJ-200 plastic scintillators are widely recognized fast scintillating materials, valued for their high light yield and mechanical robustness, which make them well suited for demanding applications in high-energy physics and space research. Their non-proportional light response, along with their non-linear behavior at low-energy X-rays, has been extensively investigated in previous studies, revealing potential systematic effects in existing measurements. In this work, light quenching in both scintillators is measured under charged-particle excitation. The results are interpreted using the modified Birks–Onsager model, which provides a theoretical framework for understanding the underlying quenching mechanisms, as well as a generalized logistic parametrization, offering experimentalists a useful tool to characterize the detector's light yield and associated uncertainties.

Keywords: quenching; LYSO; EJ200; scintillator

check for updates

Academic Editors: Matteo Duranti, Valerio Vagelli and Armen Sedrakian

Received: 1 September 2025
Revised: 19 September 2025
Accepted: 28 September 2025
Published: 30 September 2025

Citation: Dimiccoli, F.; Follega, F.M.; Ghezzer, L.E.; Iuppa, R.; Lega, A.; Nicolaidis, R.; Nozzoli, F.; Ricci, E.; Verroi, E.; Zuccon, P. A New Measurement of Light Yield Quenching in EJ-200 and LYSO Scintillators. *Particles* **2025**, *8*, 82. https://doi.org/10.3390/particles8040082

Copyright: © 2025 by the authors. Licensee MDPI, Basel, Switzerland. This article is an open access article distributed under the terms and conditions of the Creative Commons Attribution (CC BY) license (https://creativecommons.org/licenses/by/4.0/).

1. Introduction

The deviation from proportionality in the light output of both organic and inorganic scintillators, especially when energy deposition occurs under conditions of high ionization density, has been extensively reported in the literature [1]. Such behavior is one of the main sources of light yield reduction when scintillators are traversed by slow charged particles or heavy nuclei. Moreover, quenching phenomena induce non-linearities in response to low-energy X/γ radiation, mainly due to the reduced velocity of the produced secondary electrons. Large ionization densities can also originate from the simultaneous passage of many ionizing particles within the same scintillator volume; in these cases, a full characterization of detector performance must include quenching from multiple overlapping tracks. This mechanism is responsible, for example, for the saturation observed in the LYSO:Ce screens employed as electron beam monitors [2] and in sampling calorimeters subjected to multi-TeV electromagnetic showers [3]. Quenching effects also play a crucial role in contexts such as the detection of nuclear recoils from fast neutrons or in Dark Matter search experiments [4,5]. From a phenomenological standpoint, scintillation quenching can be described as the result of interactions between charged carriers (electrons and holes, which predominantly undergo non-radiative recombination) and neutral carriers (excitons, highly mobile electron–hole bound states capable of transferring energy to luminescent centers).

In this framework, two main mechanisms are identified [6]. At high excitation densities, exciton–exciton interactions transfer part of their energy to the crystal lattice in the form of phonons, thereby not contributing to scintillation light. Originally introduced by Birks [1] and later refined in [7], this process leads to a luminous efficiency (L_B) that depends on the linear ionization density (dE/dx):

$$L_B = \eta_H + \frac{1-\eta_H}{1+B(1-\eta_H)\frac{dE}{dx}} \ . \tag{1}$$

Here, B is the Birks parameter, which defines the characteristic dE/dx scale at which quenching becomes relevant. The η_H parameter represents the minimum luminous efficiency at saturation and, following the interpretation in [7], can be understood as the fraction of carriers escaping from the dense ionization core to a surrounding halo with lower ionization density. A second mechanism becomes important at lower ionization densities [8–11]. $\eta_{e/h}$ denotes the initial fraction of electrons and holes that do not form excitons. Nevertheless, some of these carriers may recombine into excitons if they remain within the Onsager radius. As a result, the exciton population can increase with higher ionization density. The associated luminous efficiency (L_O) is expressed as follows:

$$L_O = 1 - \eta_{e/h}\, e^{-\frac{dE/dx}{(dE/dx)_0}} \ , \tag{2}$$

where $(dE/dx)_0$ sets the ionization density scale governing the Onsager process. Within this simplified model, the relative light yield is proportional to the $L_B L_O$ product, which successfully describes scintillator responses to both electrons and ions, as well as the observed non-linearity for low-energy photons [12]. Despite its compact form, this description can also reproduce the temperature dependence of scintillation [13] and the deterioration of energy resolution for low-energy electron and photon detection [14,15].

It is important to emphasize that the opposite trends of Birks and Onsager quenching can lead to strong correlations among the four parameters of this generalized model. This correlation can hinder its use for performance characterization and may cause significant uncertainty when estimating the systematic contribution of quenching to detector response. For this reason, we also employ a generalized logistic model to fit experimental data:

$$L_{GL} = L_\infty + \frac{1-L_\infty}{1+\left(\frac{1}{K}\frac{dE}{dx}\right)^\alpha} \ , \tag{3}$$

which reduces to the modified Birks law (Equation (1)) when $\alpha = 1$. In this case, L_∞ and $1/K$ play the same phenomenological roles as η_H and $B(1-\eta_H)$, respectively.

2. Quenching Measurements in EJ-200 and LYSO Scintillators

The EJ-200 from Eljen Technology [16] is a versatile plastic scintillator closely related to Nuclear Enterprise's Pilot-F and Saint-Gobain BC-408. It is based on polyvinyltoluene (PVT) and incorporates proprietary wavelength-shifting fluors. Thanks to its high light output (∼10 ph./keV), long optical attenuation length (3.8 m), and fast timing (rise and decay constants of 0.9 ns and 2.1 ns, respectively), EJ-200 is widely adopted in particle-physics instrumentation. Eljen's technical notes provide a plot of the EJ-200 response for charged particles spanning different ionization densities. Complementary information is available from the Lawrence Berkeley National Laboratory Scintillator Library. The datasets reported in [16] comprise measurements of electron recoils up to 1 MeV [17] and of proton recoils up to a few MeV generated by fast-neutron exposure [18–20]. Additional studies examined the response to electrons [10] and to γ-ray sources [21]. Under the assumption of the original Birks law (i.e., setting $n_H = 0$ and $\eta_{e/h} = 0$ within the generalized framework), these

measurements report $1/B = 91$ MeV/cm [10] and $B = 0.016$ cm/MeV [21], respectively. A more recent analysis of EJ-200 exposed to relativistic nuclei [22] suggests that substantial quenching becomes evident only for $dE/dx \gtrsim 100$ MeV/cm; this does not seem compatible with all other existing measurements [23].

The second detector material considered here is cerium-doped Lutetium–Yttrium Oxyorthosilicate (LYSO:Ce). LYSO:Ce is an inorganic scintillator characterized by high density ($\sim$7.2 g/cm^3), a large effective atomic number ($Z_{\text{eff}} \sim 65$), high light yield ($\sim$30 ph./keV), and fast decay ($\tau \sim 40$ ns). These attributes (combined with good radiation hardness, relatively strong mechanical properties, and moderate cost) have led to the widespread use of LYSO in medical PET systems and high-energy physics detectors, despite its intrinsic radioactivity of about 40 Bq/g [24]. A pronounced non-proportional response to sub-MeV X/γ radiation is also well established for LYSO [25–28]. Initial measurements of LYSO with proton beams [29,30] and with heavier nuclei [31,32] extracted quenching parameters using several modified Birks-style parameterizations. More recently, dedicated measurements with a 30 GeV/n relativistic argon beam (including its fragments) have provided precise determinations of the generalized Birks–Onsager parameters for LYSO, probing ionization densities up to $\sim$4000 MeV/cm [6]. Finally, interesting results for large ionization densities have been published by RIBF/RIKEN using He, Sn, Sb, and Te ions [33]. As in the EJ-200 case, a careful comparison of published LYSO datasets reveals discrepancies in the reported quenching magnitude as a function of the linear ionization density.

3. Measurement with Charged Particles

To investigate scintillation quenching in EJ-200 and LYSO:Ce, the experimental arrangement illustrated in Figure 1 (left) was employed.

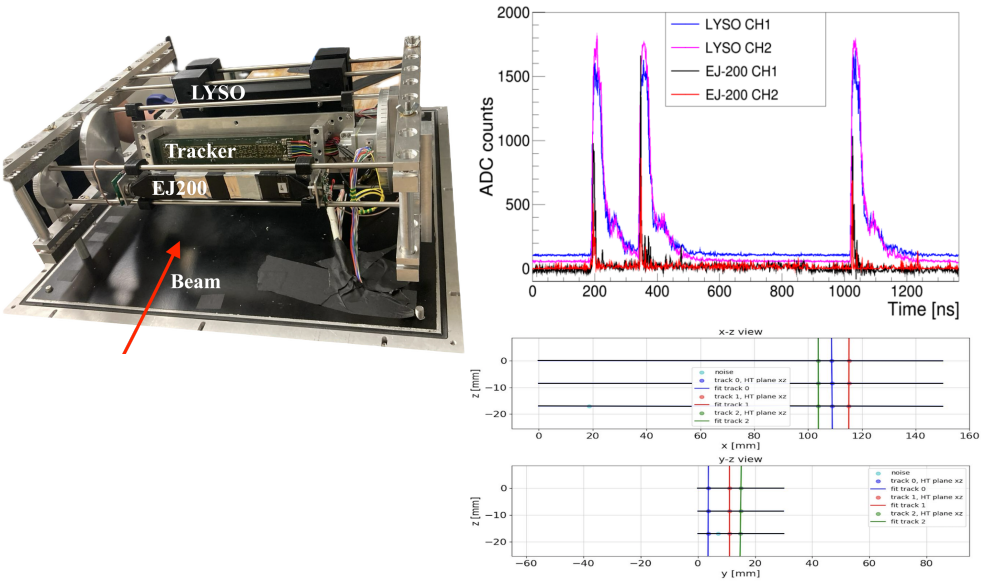


Figure 1. Left: Schematic of the setup adopted for the measurements. The EJ-200 plastic scintillator ($15 \times 3 \times 0.2$ cm^3) provided the primary trigger. A valid trigger activated the readout of both a 3-layer ALTAI silicon pixel tracker [34] and a LYSO:Ce scintillator ($15 \times 5 \times 2.5$ cm^3). Right: Example of a multiple-proton event recorded during MHz-rate data acquisition. The top panel shows the PMT waveforms, while the bottom panel displays the side views of the reconstructed tracks, revealing the pile-up of three distinct protons (the z direction is taken to be along the beam axis).

The trigger is generated by the EJ-200 scintillator (dimensions of $15 \times 3 \times 0.2$ cm^3), activating the digitization of a three-layer ALTAI silicon pixel tracker [34] and a LYSO:Ce scintillator ($15 \times 5 \times 2.5$ cm^3, mass of 1350 g, supplied by Filar Optomaterials). Each

scintillator was optically coupled at both ends to Hamamatsu R9880U-210 PMTs. The signals were recorded at 5 GS/s using a CAEN DT5742 digitizer, with the peak amplitude extracted for subsequent analysis.

A silicon tracker with a spatial pitch of ∼28 µm provided accurate reconstruction of the particle trajectories and enabled the identification or rejection of pile-up events involving more than one particle. An illustrative case is reported in Figure 1 (right), recorded with a 120 MeV proton beam under high-rate (∼MHz) conditions: both scintillators (upper plot) registered the signals from three individual protons, whose distinct tracks were resolved in the tracker side views (lower plot).

Calibration of the scintillator response and verification of readout linearity were carried out using the well-known energy loss of vertical and inclined cosmic muons (MIPs).

For the beam tests, the detectors were positioned so that the beam passed perpendicularly through 0.2 cm of EJ-200 and 2.5 cm of LYSO. Proton beams with energies between 70 and 228 MeV were delivered at the INFN/TIFPA experimental hall of the APSS Protontherapy Centre in Trento [35]. Additional measurements with 170–400 MeV/n carbon ions and 110–130 MeV protons were performed at the CNAO facility in Pavia [36]. The expected distributions of deposited energy and track length for each beam energy were estimated with Geant4 simulations [37].

Figure 2 presents the comparison between the measured energy deposition and Geant4 predictions for EJ-200 and LYSO. It is important to note that light quenching effects are not included in the Geant4 simulation of the deposited energy. For LYSO, only protons above 125 MeV and carbon ions above 2600 MeV could fully traverse the crystal. In both scintillators, the ratio of measured to simulated deposited energy decreases when the beam energy is lowered or the ion charge is increased, consistent with the expected behavior from scintillation quenching. In the case of carbon ions below ∼3 GeV, the data reveal a strong suppression of light yield despite the higher energy deposit; this is an effect similar to the "smoke-ring" effect reported in [2].

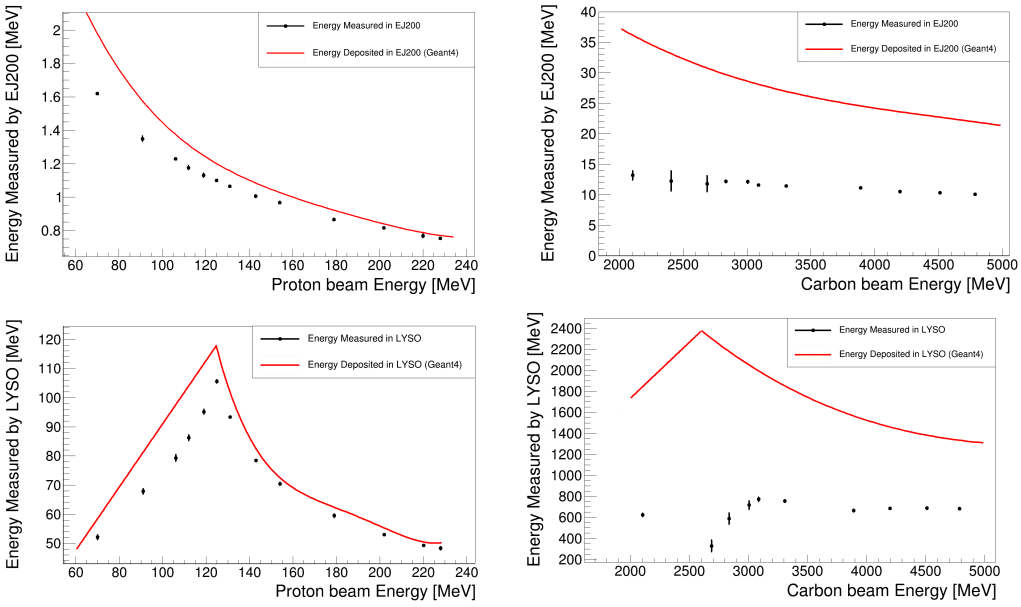


Figure 2. Deposited energy measured in the scintillators (black points) compared with Geant4 expectations (red curves). It is important to note that light quenching effects are not included in the

Geant4 simulation of the deposited energy. Top: EJ-200; bottom: LYSO. Only protons above 125 MeV and carbon ions above 2600 MeV were able to cross the entire 2.5 cm LYSO crystal. The measured-to-simulated energy ratio decreases as beam energy is reduced or particle charge is increased, in agreement with quenching effects. In the case of carbon ions below ∼3 GeV, the data reveal a strong suppression of light yield despite the higher energy deposit, this is an effect similar to the "smoke-ring" effect reported in [2].

4. Scintillation Quenching Results

To determine the light yield, the measured energy deposition (calibrated with MIPs, black points in Figure 2) was divided by the expected energy deposition (red lines in the same plots) for each scintillator sample. Figure 3 shows the light yield relative to MIPs for EJ-200 (top) and LYSO (bottom).

Magenta and blue points correspond to our proton and carbon measurements, respectively, while the black point represents the cosmic muon (MIP) reference, which sets the absolute scale. The dE/dx values were obtained from Geant4 simulations, representing the mean specific ionization density for each beam ofenergy. Additional points in the plots correspond to other light-yield measurements from the literature for EJ-200 and LYSO.

For the global EJ-200 scintillation quenching analysis, the data from [22] were excluded due to a significant discrepancy relative to all other results. The gray shaded band and gray triangles in Figure 3 (top plot) were derived from [16,20], which reported the integrated light response ($L(E)$) for stopping particles. In this case, dL/dE was obtained by differentiating $L(E)$ and averaging the specific energy loss within each energy interval. The same approach was applied to evaluate the RIBF/RIKEN data in Figure 3 (bottom plot).

Overall, a reasonable agreement among the EJ-200 datasets is observed. The "pure" Birks' law curve ($B = 0.016$ cm/MeV, red dashed line) from [21], commonly used in detector-response simulations, reproduces the measurements within ∼25%. A global fit with the Birks–Onsager model yields 1/B = 12.0 ± 1.3 MeV/cm, $\eta_{e/h}$ = 0.853 ± 0.014, and $(dE/dx)_0$ = 134 ± 6 MeV/cm, with η_H fixed to zero (black line). The generalized logistic model (Equation (3), green dotted line), which is suggested for reliable systematic-uncertainty evaluation of the EJ-200 scintillation quenching description, returns K = 65 ± 3 MeV/cm, α = 0.75 ± 0.02, and similarly to the η_H of the previous fit, L_∞ can be fixed to zero.

For LYSO, the dataset from [29,30] was discarded because it corresponds to a crystal with an unusually low density (5.4 g/cm^3) and also shows large discrepancies compared with the other measurements. Additionally, the carbon-ion dataset from Koba et al. [31,32] ($dE/dx \sim 1000$ MeV/cm, empty squares in Figure 3) also shows discrepancies with respect to all other measurements and was excluded from the global fit.

The Birks–Onsager parametrization from [6] (red line and shaded band in Figure 3 bottom) returns 1/B = 45.1 ± 9.1 MeV/cm, η_H = 0.0274 ± 0.0048, $\eta_{e/h}$ = 0.758 ± 0.045, and $(dE/dx)_0$ = 164.7 ± 8.4 MeV/cm, in reasonable agreement with (non-carbon) data from Koba et al. and RIBF/RIKEN [33], as well as our results. However, the extrapolation of [6] to high ionization density (dashed red line) fails to describe Sn, Sb, and Te data from RIBF/RIKEN.

Assuming all LYSO light-yield measurements are affected by similar dominant systematic uncertainties, the global Birks–Onsager fit for LYSO yields (black line) 1/B = 361 ± 16 MeV/cm and η_H = 0.053 ± 0.015, while $\eta_{e/h}$ is fixed at 0, since the data do not support the presence of an Onsager term. The generalized logistic fit (Equation (3), green dotted line) yields K = 380 ± 15 MeV/cm, α = 1.00 ± 0.04, and L_∞ = 0.050 ± 0.011; therefore, it supports the modified Birks ($\alpha \equiv 1$) parametrization.

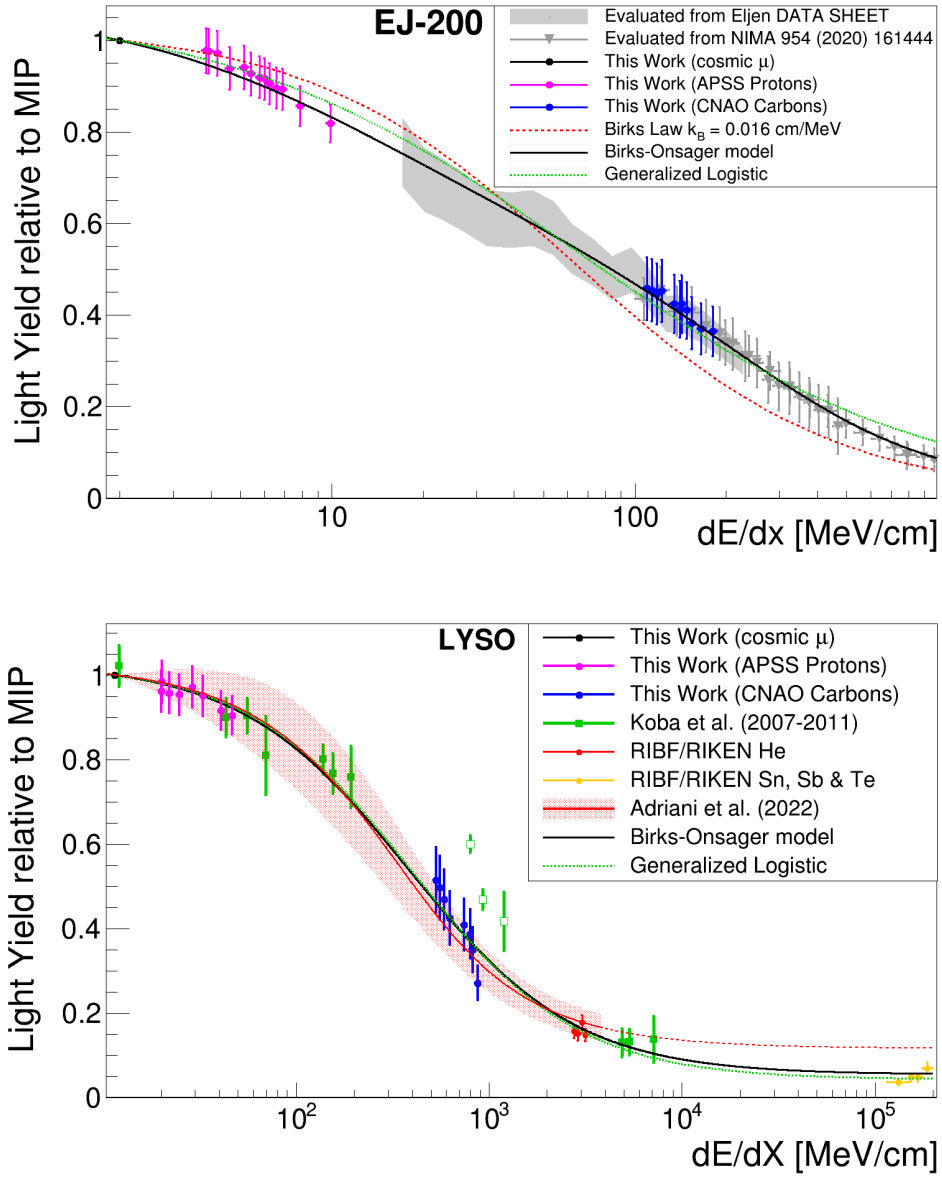


Figure 3. Light yield relative to MIPs. Black point: cosmic muons; magenta and blue points: proton and carbon beam measurements, respectively (APSS and CNAO). Top plot (EJ-200): black solid line is the Birks–Onsager best fit (1/B = 12.0 ± 1.3 MeV/cm, $\eta_{e/h}$ = 0.853 ± 0.014, $(dE/dx)_0$ = 134 ± 6 MeV/cm, $\eta_H \equiv 0$); green dotted line is the generalized logistic fit (K = 65 ± 3 MeV/cm, α = 0.75 ± 0.02, $L_\infty \equiv 0$). Literature data from [16,20] and the "pure" Birks' law curve ($B = 0.016$cm/MeV, red dashed line) [21] are also shown. Bottom plot (LYSO): black solid line is the Birks–Onsager best fit: 1/B = 361 ± 16 MeV/cm, η_H = 0.053 ± 0.015, while $\eta_{e/h}$ was fixed at 0, since data do not support the presence of an Onsager term; green dotted line is the generalized logistic fit (K = 380 ± 15 MeV/cm, α = 1.00 ± 0.04, L_∞ = 0.050 ± 0.011). Literature data from [31–33] and the Birks–Onsager parametrization from [6] (1/B = 45.1 ± 9.1 MeV/cm, η_H = 0.0274 ± 0.0048, $\eta_{e/h}$ = 0.758 ± 0.045, $(dE/dx)_0$ = 164.7 ± 8.4 MeV/cm, red line with shaded band) are also shown.

5. Conclusions

In this work, we investigated scintillation quenching in EJ-200 and LYSO:Ce using charged particle beams and cosmic muons.

For EJ-200, the Birks–Onsager model provided a good description of the data, yielding 1/B = 12.0 ± 1.3 MeV/cm, $\eta_{e/h}$ = 0.853 ± 0.014, and $(dE/dx)_0$ = 134 ± 6 MeV/cm, with η_H fixed to zero.

For LYSO, the combination of our measurements and literature data is described by the simple modified Birks model: $1/B = 361 \pm 16$ MeV/cm and $\eta_H = 0.053 \pm 0.015$, while $\eta_{e/h}$ is fixed at 0, since the data do not support the presence of an Onsager term.

Despite the Birks–Onsager model being theoretically well motivated, we propose using a generalized logistic fit to reduce degeneracy in the parameters. For EJ-200, the fit yielded $K = 65 \pm 3$ MeV/cm, $\alpha = 0.75 \pm 0.02$, and $L_\infty \equiv 0$, providing a description of the quenching behavior that is most suitable for experimentalists. For LYSO, the generalized logistic fit yielded $K = 380 \pm 15$ MeV/cm, $\alpha = 1.00 \pm 0.04$, and $L_\infty = 0.050 \pm 0.011$, showing that even a simple modified Birks model can reasonably describe the dataset.

Finally, we note that measurements of the light yield in EJ-200 for $dE/dx > 800$ MeV/cm and in LYSO for $dE/dx > 3000$ MeV/cm are scarce; thus, sizable systematic uncertainties in the determination of the L_∞ (or η_H) parameters are possible. A dedicated experiment using α particles from ^{241}Am is currently ongoing at the INFN/TIFPA laboratory to further probe EJ-200 and LYSO light yield in this extreme ionization density regime.

Author Contributions: Conceptualization, R.I., A.L., and F.N.; methodology, R.I., A.L., and F.N.; software, A.L. and F.N.; validation, A.L., F.N., and R.I.; formal analysis, F.N. and A.L.; investigation, F.M.F., L.E.G., R.I., A.L., R.N., F.N., E.R., E.V., and P.Z.; resources, R.I. and F.N.; data curation, A.L., L.E.G., and F.N.; writing—original draft preparation, F.D., F.M.F., L.E.G., R.I., A.L., R.N., F.N., E.R., E.V., and P.Z.; writing—review and editing, F.D., F.M.F., L.E.G., R.I., A.L., R.N., F.N., E.R., E.V., and P.Z.; visualization, A.L. and L.E.G.; supervision, F.N. and R.I.; project administration, F.N. and R.I.; funding acquisition, F.N., R.I., and P.Z. All authors have read and agreed to the published version of the manuscript.

Funding: This research received no external funding.

Data Availability Statement: The raw data supporting the conclusions of this article will be made available by the authors on request.

Acknowledgments: We thank Veronica Vilona for her support in organizing and performing the test beam.

Conflicts of Interest: The authors declare no conflicts of interest.

Abbreviations

The following abbreviations are used in this manuscript:

LYSO	Lutetium–yttrium oxyorthosilicate
MIP	Minimum Ionizing Particle
PMT	Photomultiplier Tube

References

1. Birks, J.B. *The Theory and Practice of Scintillation Counting: International Series of Monographs in Electronics and Instrumentation*; Elsevier: Amsterdam, The Netherlands, 2013; Volume 27.
2. Kube, G.; Liu, S.; Novokshonov, A.; Scholz, M. Identification and Mitigation of Smoke-Ring Effects in Scintillator-Based Electron Beam Images at the European XFEL. In Proceedings of the FEL'19 39th Free Electron Laser Conference, Hamburg, Germany, 26–30 August 2019; JACoW Publishing: Geneva, Switzerland, 2019; pp. 301–306. [CrossRef]
3. Kounine, A.; Weng, Z.; Xu, W.; Zhang, C. Precision measurement of 0.5GeV–3TeV electrons and positrons using the AMS Electromagnetic Calorimeter. *Nucl. Instrum. Methods Phys. Res. Sect. A Accel. Spectrometers Detect. Assoc. Equip.* **2017**, *869*, 110–117. [CrossRef]
4. Tretyak, V. Semi-empirical calculation of quenching factors for ions in scintillators. *Astropart. Phys.* **2010**, *33*, 40–53. [CrossRef]
5. Tretyak, V.I. Semi-empirical calculation of quenching factors for scintillators: New results. *EPJ Web Conf.* **2014**, *65*, 02002. [CrossRef]
6. Adriani, O.; Berti, E.; Betti, P.; Bigongiari, G.; Bonechi, L.; Bongi, M.; Bottai, S.; Brogi, P.; Castellini, G.; Checchia, C.; et al. Light yield non-proportionality of inorganic crystals and its effect on cosmic-ray measurements. *J. Instrum.* **2022**, *17*, P08014. [CrossRef]

7. Tarle, G.; Ahlen, S.P.; Cartwright, B.G. Cosmic ray isotope abundances from chromium to nickel. *ApJ* **1979**, *230*, 607–620. [CrossRef]
8. Moses, W.W.; Payne, S.A.; Choong, W.S.; Hull, G.; Reutter, B.W. Scintillator Non-Proportionality: Present Understanding and Future Challenges. *IEEE Trans. Nucl. Sci.* **2008**, *55*, 1049–1053. [CrossRef]
9. Payne, S.A.; Cherepy, N.J.; Hull, G.; Valentine, J.D.; Moses, W.W.; Choong, W.S. Nonproportionality of Scintillator Detectors: Theory and Experiment. *IEEE Trans. Nucl. Sci.* **2009**, *56*, 2506–2512. [CrossRef]
10. Payne, S.A.; Moses, W.W.; Sheets, S.; Ahle, L.; Cherepy, N.J.; Sturm, B.; Dazeley, S.; Bizarri, G.; Choong, W.S. Nonproportionality of Scintillator Detectors: Theory and Experiment. II. *IEEE Trans. Nucl. Sci.* **2011**, *58*, 3392–3402. [CrossRef]
11. Payne, S.; Hunter, S.; Sturm, B.; Cherepy, N.; Ahle, L.; Sheets, S.; Dazeley, S.; Moses, W.; Bizarri, G. Physics of scintillator nonproportionality. In Proceedings of the Hard X-Ray, Gamma-Ray, and Neutron Detector Physics XIII, San Diego, CA, USA, 22–24 August 2011; Volume 8142, pp. 251–257.
12. Beck, P.R.; Payne, S.A.; Hunter, S.; Ahle, L.; Cherepy, N.J.; Swanberg, E.L. Nonproportionality of Scintillator Detectors. V. Comparing the Gamma and Electron Response. *IEEE Trans. Nucl. Sci.* **2015**, *62*, 1429–1436. [CrossRef]
13. Payne, S.A.; Hunter, S.; Ahle, L.; Cherepy, N.J.; Swanberg, E. Nonproportionality of Scintillator Detectors. III. Temperature Dependence Studies. *IEEE Trans. Nucl. Sci.* **2014**, *61*, 2771–2777. [CrossRef]
14. Iredale, P. The effect of the non-proportional response of NaI(Tl) crystals to electrons upon the resolution for γ-rays. *Nucl. Instrum. Methods* **1961**, *11*, 340–346. [CrossRef]
15. Payne, S.A. Nonproportionality of Scintillator Detectors. IV. Resolution Contribution from Delta-Rays. *IEEE Trans. Nucl. Sci.* **2015**, *62*, 372–380. [CrossRef]
16. Eljen Technology: Response of EJ-200 Plastic Scintillator and Berkeley National Laboratory Scintillator Library. Available online: https://eljentechnology.com/images/technical_library/EJ200_Resp.pdf (accessed on 10 April 2025).
17. Swiderski, L.; Marcinkowski, R.; Moszynski, M.; Czarnacki, W.; Szawlowski, M.; Szczesniak, T.; Pausch, G.; Plettner, C.; Roemer, K. Electron response of some low-Z scintillators in wide energy range. *J. Instrum.* **2012**, *7*, P06011. [CrossRef]
18. Langford, T.; Beise, E.; Breuer, H.; Heimbach, C.; Ji, G.; Nico, J. Development and characterization of a high sensitivity segmented Fast Neutron Spectrometer (FaNS-2). *J. Instrum.* **2016**, *11*, P01006. [CrossRef] [PubMed]
19. Tkaczyk, A.; Saare, H.; Ipbüker, C.; Schulte, F.; Mastinu, P.; Paepen, J.; Pedersen, B.; Schillebeeckx, P.; Varasano, G. Characterization of EJ-200 plastic scintillators as active background shield for cosmogenic radiation. *Nucl. Instrum. Methods Phys. Res. Sect. A Accel. Spectrometers Detect. Assoc. Equip.* **2018**, *882*, 96–104. [CrossRef]
20. Laplace, T.; Goldblum, B.; Brown, J.; Bleuel, D.; Brand, C.; Gabella, G.; Jordan, T.; Moore, C.; Munshi, N.; Sweger, Z.; et al. Low energy light yield of fast plastic scintillators. *Nucl. Instrum. Methods Phys. Res. Sect. A Accel. Spectrometers Detect. Assoc. Equip.* **2020**, *954*, 161444. [CrossRef]
21. Tajudin, S.M.; Namito, Y.; Sanami, T.; Hirayama, H. Response of plastic scintillator to gamma sources. *Appl. Radiat. Isot.* **2020**, *159*, 109086. [CrossRef] [PubMed]
22. Loizzo, P.; Cerasole, D.; Barbato, F.; Bissaldi, E.; Cagnoli, I.; Casilli, E.; De Mitri, I.; De Palma, F.; Di Giovanni, A.; Di Venere, L.; et al. Characterization of light yield non-proportionality in plastic scintillator-based detectors for satellite cosmic-ray experiments. *Nucl. Instrum. Methods Phys. Res. Sect. A Accel. Spectrometers Detect. Assoc. Equip.* **2024**, *1069*, 169888. [CrossRef]
23. Nozzoli, F. A New Measurement of Light Yield Quenching in EJ-200 and LYSO Scintillators. Poster Presented at ASAPP2025. Available online: https://indico.cern.ch/event/1463191/contributions/6434257/ (accessed on 29 September 2025).
24. Ghezzer, L.E.; Nozzoli, F.; Nicolaidis, R.; De Santis, C.; Iuppa, R.; Zuccon, P. Search for electron capture in Lu176 with a lutetium yttrium oxyorthosilicate scintillator. *Phys. Rev. C* **2023**, *107*, 045504. [CrossRef]
25. Pepin, C.; Berard, P.; Perrot, A.L.; Pepin, C.; Houde, D.; Lecomte, R.; Melcher, C.; Dautet, H. Properties of LYSO and recent LSO scintillators for phoswich PET detectors. *IEEE Trans. Nucl. Sci.* **2004**, *51*, 789–795. [CrossRef]
26. Chewpraditkul, W.; Swiderski, L.; Moszynski, M.; Szczesniak, T.; Syntfeld-Kazuch, A.; Wanarak, C.; Limsuwan, P. Scintillation Properties of LuAG:Ce, YAG:Ce and LYSO:Ce Crystals for Gamma-Ray Detection. *IEEE Trans. Nucl. Sci.* **2009**, *56*, 3800–3805. [CrossRef]
27. Wanarak, C.; Chewpraditkul, W.; Phunpueok, A. Light yield non-proportionality and energy resolution of $Lu_{1.95}Y_{0.05}SiO_5$: Ce and Lu_2SiO_5: Ce scintillation crystals. *Procedia Eng.* **2012**, *32*, 765–771. [CrossRef]
28. Khodyuk, I.V.; Dorenbos, P. Trends and Patterns of Scintillator Nonproportionality. *IEEE Trans. Nucl. Sci.* **2012**, *59*, 3320–3331. [CrossRef]
29. So, J.; Kim, H.; Kang, H.; Park, H.; Lee, S.; Kim, S.; Kim, K.; Lee, M. The Proton Energy Response of a LYSO Crystal. *J. Korean Phys. Soc.* **2008**, *52*, 925–929. [CrossRef]
30. Sang, J.K.; MinJeong, K.; Jeongmin, P.; Jooyoung, L.; Jukyung, S.; DaeHoon, H.; Yongseok, H. Measurement of the Proton Luminescence Response and Determination of the Birks Parameters of the LYSO Crystal. *New Phys. Sae Mulli* **2016**, *66*, 679–684. [CrossRef]

31. Koba, Y.; Wakabayashi, G.; Imamura, M.; Uozumi, Y.; Koba, N.; Iwamoto, H.; Ohkawa, H.; Shimazu, T.; Matsufuji, N.; Evtoukhovitch, P.; et al. Light output response of LYSO(Ce) crystal to relativistic helium and carbon ions. In Proceedings of the 2007 IEEE Nuclear Science Symposium Conference Record, Honolulu, HI, USA, 26 October–3 November 2007; Volume 3, pp. 2303–2306. [CrossRef]
32. Koba, Y.; Iwamoto, H.; Kiyohara, K.; Nagasaki, T.; Wakabayashi, G.; Uozumi, Y.; Matsufuji, N. Scintillation efficiency of inorganic scintillators for intermediate-energy charged particles. *Prog. Nucl. Sci. Technol.* **2011**, *1*, 218–221. [CrossRef]
33. Kreider, B.; Cox, I.; Grzywacz, R.; Allmond, J.M.; Augustyn, A.; Braukman, N.; Brionnet, P.; Esmaylzadeh, A.; Fischer, J.; Fukuda, N.; et al. Modeling of Light Production in Inorganic Scintillators. *arXiv* **2025**. [CrossRef]
34. Ricci, E. First use of Monolithic Active Pixel Sensors for tracking particles in space. In Proceedings of the 44th COSPAR Scientific Assembly, Athens, Greece, 16–24 July 2022; Volume 44, p. 3057.
35. Tommasino, F.; Rovituso, M.; Fabiano, S.; Piffer, S.; Manea, C.; Lorentini, S.; Lanzone, S.; Wang, Z.; Pasini, M.; Burger, W.; et al. Proton beam characterization in the experimental room of the Trento Proton Therapy facility. *Nucl. Instrum. Methods Phys. Res. Sect. A Accel. Spectrometers Detect. Assoc. Equip.* **2017**, *869*, 15–20. [CrossRef]
36. Giordanengo, S.; Garella, M.A.; Marchetto, F.; Bourhaleb, F.; Ciocca, M.; Mirandola, A.; Monaco, V.; Hosseini, M.A.; Peroni, C.; Sacchi, R.; et al. The CNAO dose delivery system for modulated scanning ion beam radiotherapy. *Med. Phys.* **2015**, *42*, 263–275. [CrossRef]
37. Allison, J.; Amako, K.; Apostolakis, J.; Arce, P.; Asai, M.; Aso, T.; Bagli, E.; Bagulya, A.; Banerjee, S.; Barrand, G.; et al. Recent developments in Geant4. *Nucl. Instrum. Methods Phys. Res. Sect. A Accel. Spectrometers Detect. Assoc. Equip.* **2016**, *835*, 186–225. [CrossRef]

Disclaimer/Publisher's Note: The statements, opinions and data contained in all publications are solely those of the individual author(s) and contributor(s) and not of MDPI and/or the editor(s). MDPI and/or the editor(s) disclaim responsibility for any injury to people or property resulting from any ideas, methods, instructions or products referred to in the content.